eNeuro

Research Article: New Research | Disorders of the Nervous System

Synaptic Actions of Amyotrophic-Lateral-Sclerosis-Associated G85R-SOD1 in the Squid Giant Synapse

https://doi.org/10.1523/ENEURO.0369-19.2020

Cite as: eNeuro 2020; 10.1523/ENEURO.0369-19.2020

Received: 14 September 2019
Revised: 22 January 2020
Accepted: 27 January 2020

Manuscript Title Page

1. Manuscript Title (50 word maximum)

Synaptic Actions of Amyotrophic-Lateral-Sclerosis-Associated G85R-SOD1 in the Squid Giant Synapse

2. Abbreviated Title (50 character maximum) Synaptic Actions of ALS-Associated-G85R-SOD1

3. List all Author Names and Affiliations in order as they would appear in the published article

Yuyu Song[1,2,3,4]

1. Department of Genetics, Yale School of Medicine, Howard Hughes Medical Institute, New Haven, CT 06510, USA
2. Laboratory of Systems Pharmacology, Program in Therapeutic Science, Harvard Medical School, Boston, MA 02115, USA
3. Department of Neurology, Massachusetts General Hospital, Charlestown, MA, 02129, USA
4. Marine Biological Laboratory, Woods Hole, MA 02543, USA

4. Author Contributions:

YS contributed to the conception of ideas, design and performance of experiments, analysis and curation of data, as well as generation and submission of the manuscript.

5. Correspondence should be addressed to (include email address)

Yuyu Song
Yuyu_Song@hms.harvard.edu, ysong13@mgh.harvard.edu

6. Number of Figures 12
7. Number of Tables 0
8. Number of Multimedia 0
9. Number of words for Abstract 190
10. Number of words for Significance Statement 120
11. Number of words for Introduction 864
12. Number of words for Discussion 2719

13. Acknowledgements

This project was supported generously by the Grass Foundation, Howard Hughes Medical Institute, and multiple awards from Harvard Medical School and Massachusetts General Hospital. The author would like to sincerely thank Drs. Arthur Horwich, George Augustine, Scott Brady, Rodolfo Llinas, Wayne Fenton for their valuable suggestions and critical evaluation of the experiments and the final manuscript. SOD1 proteins were gifts from the Horwich laboratory, prepared by Drs. Weiming Ni and Wayne Fenton. The author also received tremendous help from Drs. Jorge E. Moreira and Pri Comassio with EM data acquisition and analysis.

14. Conflict of Interest

No The authors declare no conflict of interest.

15. Funding sources
Grass Foundation, HHMI, MGH Jack Satter Foundation, Harvard University ALS and Alzheimer's Endowed Research Fund, Harvard Brain Science Initiative.

ABSTRACT (190 words)

Altered synaptic function is thought to play a role in many neurodegenerative diseases, but little is known about the underlying mechanisms for synaptic dysfunction. The squid giant synapse (SGS) is a classical model for studying synaptic electrophysiology and ultrastructure, as well as molecular mechanisms of neurotransmission. Here, we conduct a multidisciplinary study of synaptic actions of misfolded human G85R-SOD1 causing familial Amyotrophic Lateral Sclerosis (fALS). G85R-SOD1, but not WT-SOD1, inhibited synaptic transmission, altered presynaptic ultrastructure, and reduced both the size of the Readily Releasable Pool (RRP) of synaptic vesicles and mobility from the Reserved Pool (RP) to the RRP. Unexpectedly, intermittent high frequency stimulation (iHFS) blocked inhibitory effects of G85R-SOD1 on synaptic transmission, suggesting aberrant Ca^{2+} signaling may underlie G85R-SOD1 toxicity. Ratiometric Ca^{2+} imaging showed significantly increased presynaptic Ca^{2+} induced by G85R-SOD1 that preceded synaptic dysfunction. Chelating Ca^{2+} using EGTA prevented synaptic inhibition by G85R-SOD1, confirming the role of aberrant Ca^{2+} in mediating G85R-SOD1 toxicity. These results extended earlier findings in mammalian motor neurons and advanced our understanding by providing possible molecular mechanisms and therapeutic targets for synaptic dysfunctions in ALS as well as a unique model for further studies.

SIGNIFICANCE STATEMENT

The squid giant synapse presents one of the few mature nervous systems *in situ* that mimics mammalian neuromuscular junctions, while allowing precise experimental manipulations and live measurement with superior spatial and temporal resolution. Applying these unique features to studying the molecular mechanisms of ALS, a devastating adult-onset neurodegenerative disease without cure, offers clues to understand the pathogenesis of the disease. Our results demonstrating synaptic dysfunction caused by ALS-associated mutant SOD1 protein and its underlying molecular pathways may suggest a novel

approach to an effective therapeutic intervention as well as identify biomarkers for early diagnosis. Furthermore, the altered synaptic vesicle behavior and Ca^{2+} dynamics revealed through the perturbation of neurotransmission by ALS extends our understanding of fundamental synaptic physiology at both molecular and cellular levels.

INTRODUCTION

ALS is a fatal adult-onset neuromuscular disease with dysfunction and loss in both upper and lower motor neurons, resulting in progressive muscle weakness and atrophy, eventual paralysis, and death usually within 3-5 years after initial diagnosis. Inherited forms of ALS represent roughly 10% of cases, with similar clinical symptoms to sporadic ALS patients. Unfortunately, there is still no effective cure for ALS. To enable therapeutic intervention at an early stage of the disease, the mechanisms underlying ALS and presymptomatic biomarkers for early diagnosis must be identified.

Mutations in Cu/Zn superoxide dismutase (SOD1) are responsible for ~25% of familial ALS cases, but SOD1 is expressed in many cell types where it removes superoxide radicals and is a component of redox signaling pathways. ALS-associated mutations induce a conformational change within SOD1 due to protein misfolding (Bruijn et al. 1998) and aberrant interactions with other proteins (Pasinelli et al. 2004; Urushitani et al. 2006). Genetic knock-out of SOD1 does not produce motor deficits seen in ALS, indicating that SOD1 mutations confer a toxic gain-of-function (Taylor, Brown, and Cleveland 2016; Ghasemi and Brown 2018; Bunton-Stasyshyn et al. 2015). A glycine-to-arginine substitution at residue 85 (G85R) is one highly studied ALS-associated mutation: G85R-SOD1 is incapable of dimerizing normally and instead misfolds into soluble monomers or oligomers, as well as insoluble aggregates that are toxic to motor neurons (Wang, Farr, Zeiss, et al. 2009; Wang, Farr, Hall, et al. 2009).

To characterize G85R-SOD1 toxicity, various forms of misfolded G85R-SOD1-YFP were perfused into isolated axoplasm from squid giant axons (Song et al. 2013), and both soluble monomers and oligomers inhibited axonal transport from cell body to synapse through aberrant activation of signaling

pathways (Song et al. 2013). Although G85R-SOD1 inhibition of anterograde transport of synaptic components could lead to synaptic dysfunction, questions remained as to whether G85R-SOD1 has a direct effect on synaptic transmission. Impairment of neuromuscular junctions is detected early in patients and animal models (Moloney, de Winter, and Verhaagen 2014), consistent with a "dying-back" neuropathy where synaptic dysfunction and loss is a primary pathology eventually leading to neuronal death. Decreased synaptic vesicle numbers and reduced presynaptic proteins in presynaptic terminals of several ALS animal models further suggest a presynaptic effect (Wang, Farr, Hall, et al. 2009). These changes are seen before motor deficits are detectable, suggesting that synapses could be a primary target of G85R-SOD1 (Sakowski et al. 2012; Hegedus, Putman, and Gordon 2007; Frey et al. 2000; Fischer et al. 2004).

Synaptic transmission is altered in ALS mouse models and iPSC-derived motor neurons, raising key questions: How do ALS-associated proteins alter synaptic functions? Can synaptic function be restored? Unfortunately, the complexity of mouse motor systems, chronic nature of disease pathology, small size of presynaptic domains, and difficulty of targeting synapses limit utility of mouse and cell culture models in addressing questions about presynaptic mechanisms.

The squid giant synapse, which mimics neuromuscular junctions with similar ion channel compositions and neurotransmission machinery (Katz and Miledi 1977, 1967), was used to evaluate pre- and post-synaptic actions of G85R-SOD1. The large size of squid giant presynaptic terminals permits experimental manipulations such as protein microinjection, direct electrophysiological measurements of transmission, current and voltage clamping, and Ca^{2+} imaging, facilitating detailed studies of presynaptic molecular mechanisms (Bloedel et al. 1966; Fukuda et al. 1995; Lin et al. 1990; Llinas et al. 1985; Llinas, Steinberg, and Walton 1980; Llinas, Sugimori, and Silver 1994; Sugimori et al. 1998; Augustine 1990; Augustine and Charlton 1986; Augustine, Charlton, and Horn 1988; Augustine et al. 2006). The squid synapse is particularly suitable for studying ALS, because it is (1) fast-transmitting with high release

capacity, similar to synapses affected in ALS; and (2) enriched in ion channels (e.g. Ca^{2+}), neurotransmitters (e.g. glutamate) and receptors (e.g. AMPAR) implicated in ALS pathology.

Here, we microinjected G85R-SOD1 in presynaptic terminals, recorded both pre- and post-synaptic membrane potentials with and without high-frequency-stimulations (HFS), performed live ratiometric Ca^{2+} imaging, and examined synaptic vesicle morphology/distribution by Electron Microscopy (EM). Correlated functional and structural studies demonstrated the acute synaptic inhibition by G85R-SOD1 as evidenced by diminished postsynaptic potentials (PSP), decreased synaptic vesicle number at active zones, and reduced synaptic mobilization from reserved (RP) to readily releasable pool (RRP) within 30min after G85R-SOD1 injection. Unexpectedly, while continuous trains of high frequency stimulation (HFS) depleted synaptic vesicle availability and enhanced synaptic inhibition by G85R-SOD1, intermittent HFS (iHFS) applied every 30min before and during G85R-SOD1 infusion kept synapses firing normally for 7h. Given the effects of HFS on presynaptic Ca^{2+}, we tested for aberrant Ca^{2+} signaling by ratiometric Ca^{2+} imaging with presynaptic Fura-2. Ca^{2+} increased throughout terminals including in "palm" regions before presynaptic axons branch, which lack plasmalemmal Ca^{2+} channels. Reducing intracellular Ca^{2+} by EGTA rescued synaptic function and restored normal structure in the presence of G85R-SOD1 as did iHFS. These results are consistent with and extend findings in mammalian nervous systems where neurons with lower Ca^{2+} buffering capacity are selectively affected in ALS and these neurons showed Ca^{2+} imbalances presymptomatically (Grosskreutz, Van Den Bosch, and Keller 2010). Understanding sources of increased Ca^{2+} and molecular mechanisms underlying Ca^{2+} activation as well as how iHFS rescues synaptic function will provide unique insights into synaptic dynamics and a possible molecular basis for synaptic pathology in human ALS patients.

MATERIALS AND METHODS

Proteins and Reagents

G85R-SOD1-His, WT-SOD1-His, G85R-SOD1-His-YFP, WT-SOD1-His-YFP were produced in *E.Coli* BL21/DE3 cells under pET vectors, and purified on Talon resin first and then by chromatography on MonoQ 10/10, in the Horwich Laboratory as described previously (Song et al. 2013). All chemicals used were American Chemical Society quality or better, from Sigma and Molecular Probes (now Fisher-Scientific). For microinjection, proteins and reagents were dissolved in 200mM KCl, 100mM Taurine, 250mM K-isethionate, 50mM K-Hepes, pH 7.4). Tetramethylrhodamine-dextran (3 kDa, Molecular Probes) was used for co-injection with non-fluorescent reagents to visualize and monitor the injection.

Squid Giant Synapse preparation and electrophysiology setup

The giant squid synapse is formed between the terminal finger of 2nd order axons of the pre-nerve and the 3rd order axon of the last stellate nerve, which is the giant axon used for axonal transport studies as well as for classical voltage-clamp studies of ion channels (Young and Keynes 2005). Following a standard protocol (Augustine 1990; Augustine and Charlton 1986; Augustine, Charlton, and Horn 1988; Augustine et al. 2006; Llinas et al. 1985; Llinas, Steinberg, and Walton 1980, 1981; Llinas, Sugimori, and Silver 1994; Smith et al. 1993), stellate ganglia of small female *Loligo pealeii* (**RRID: SCR_002864**, Marine Biological Laboratory, Woods Hole, Massachusetts) were removed from the mantle carefully and rapidly under running seawater, tied off at each end of the presynaptic and postsynaptic axons, isolated from the sheath and connective tissues, pinned with fine cactus needles to a thin-layer of Sylgard on the bottom of a 35mm Petri dish chamber, superfused continuously with oxygenated squid saline (455mM NaCl, 54mM MgCl2, 11mM CaCl2, 10mM KCl, 3mM NaHCO3, and 10mM Hepes, pH 7.2) at 10-15^{o}C.

The most distal digit of the presynaptic axons and the most medial fiber, also known as the giant axon, form the giant synapse (Figure 1A). One microelectrode for injecting was inserted in the presynaptic axon to inject current at 0.033 Hz for basal stimulation and at 50 Hz for HFS (each pulse is 2μA for 2ms for basal stimulation and 2μA for 1ms for HFS), near the "palm" where the 2nd order axon enters the ganglion to branch and form multiple synapses with postsynaptic axons. At the terminal of the most medial branch, a 2nd microelectrode was inserted to presynaptically inject proteins and reagents of

interest as well as recording the presynaptic membrane potentials. Finally, at the postsynaptic terminal of the giant synapse, a 3rd microelectrode was inserted near the medial presynaptic digit to record the postsynaptic membrane potentials. Electrodes 1 and 3 were filled with 3M KCl while the 2nd microelectrode, through which 50µM SOD1 proteins or reagents of interest were injected in 100mM KCl (Smith et al. 1993) at 0.1 Hz (each injection was 50 psi for 250 ms). The injection efficiency of SOD1 proteins was monitored by a fluorescence microscope. All synapses were injected with the same pressure for the same amount of time during data acquisition, and the final mean fluorescence intensities in the presynaptic terminals were measured and compared between samples to ensure comparable levels of infused proteins.

Electrophysiology data acquisition and analysis

Both presynaptic and postsynaptic potentials (PSP) were recorded using sharp microelectrodes with an Axoclamp-2A amplifier (Axon Instrument, Foster City, CA) and data analyzed using Labview (National Instruments) software (Yulong Li). Raw waveforms were used to calculate PSP slope using the same parameters for all experiments. For data acquired under HFS, PSP slopes were analyzed, integrated, plotted, and fitted linearly using the last 50 time points to derive the vesicle mobilization rate (slope of the linear fit) and the readily releasable pool (RRP) size (intersection with the Y axis).

Ratiometric Ca^{2+} imaging

1mM Fura-2 (pentapotassium salt, ThermoFisher F1200, CHEBI:52081), a Ca^{2+} indicator, was dissolved in 100mM KCl and infused into the presynaptic terminal by electrophoresis (100 nA current) through the 1st presynaptic electrode inserted in the "palm". Fura-2 infusion continued for 10min and the synapse was allowed to equilibrate for 30 min before presynaptic injection of SOD1 proteins through the 2nd microelectrode to ensure Fura-2 was diffused evenly throughout the whole presynaptic terminal at roughly 100µM. Ratiometric live Ca^{2+} imaging was performed every 30 seconds with ratiometric images taken at Ex360 nm and Ex390 nm assisted by an ultra-high-speed wavelength switching Lambda DG-4/5

xenon arc lamp system. Ratios at various locations (A) were calculated as (fluorescent intensity^{360nm})/(fluorescent intensity^{390nm}) as a measure of intracellular Ca^{2+} concentration (Smith et al. 1993). In vitro calibration was performed by mixing squid axoplasm with equal volumes of buffer containing 5μM Fura-2, 400mM KCl, and 40mM Na-HEPES (pH 7.2). 3 doses of $CaCl_2$ were set by adding 20mM EGTA (low Ca^{2+}, $<10^{-8}$ M), or 20mM EGTA + 13.3 mM $CaCl_2$ (intermediate Ca^{2+}, ~6.7 x 10^{-7} M), or 20mM $CaCl_2$ (high Ca^{2+}). Various ratios under each condition were measured using the same optics and the background noise was subtracted. The dose response curve was obtained to allow the determination of Kd' and the two ratios. Rmax was defined as the ratio value at saturating Ca^{2+} level, and Rmin was defined as the ratio value at the minimal Ca^{2+} concentration.

Electron Microscopy (EM)

After recordings, synapses were fixed in 4% glutaraldehyde and 2% paraformaldehyde in 0.1M cacodylate buffer for 12 hours at 4°C, then washed in 0.1M cacodylate buffer 3 times and post-fixed in 1% Osmium Tetroxide for 2 hours at 4°C, followed by blocking impregnation with 2% uranyl acetate in 0.1M sodium acetate, pH 5.0 for 24 hours. After washing, dehydration was performed in ethanol with increasing concentration: 50% for 10min, 75% for 10min, 80% for 10min, 85% for 10min, 95% for 10min, 100% for 5min twice, followed by propylene oxide for 5min three times. Resin and propylene (1:1 for 24 hours, 2:1 overnight, and 3:1 for 2-4 hours, and finally 100% resin overnight) infiltration was carried out before embedding in silicone molds in the oven at 62 °C for 72 hours. Sectioning and imaging were performed following standard EM protocols (Moreno et al. 2009; Augustine et al. 2006). Vesicle density at the active zones was determined as the number of vesicles per μm^2. Distance between vesicles and active zones was measured and plotted as described previously (Morgan et al. 1999). All EM samples were numbered, processed, and analyzed under blinded conditions till the last step when data had to be pooled.

Statistical Information.

All experiments were repeated at least five times. The data were analyzed by one-way ANOVA followed by the Tukey *post-hoc* test (or nonparametric multiple t-tests, without assuming consistent SD) and plotted in Prism 7 (GraphPad software). Quantitative data were plotted as mean ± SEM. P values were calculated and four statistical thresholds were marked: P<0.00001, P<0.0001, P<0.001 and P<0.005 (P<0.05 indicated statistical significance). For EM analysis, nested one-way ANOVA was performed to compare WT and G85R infused synapses (102 synapses across 3 synapses for each group).

RESULTS

G85R-SOD1-YFP but not WT-SOD1-YFP inhibits synaptic transmission

To assess whether the mutant SOD1 is directly toxic to the synapse, as opposed to indirectly affecting it, e.g. by blocking axonal anterograde vesicular trafficking (Song et al. 2013), G85R-SOD1-YFP (*n = 8*) or WT-SOD1-YFP control (*n = 5*) was microinjected in the presynaptic terminal site (Fig.1A) through the micropipette extending in from lower right; note that black color indicates the extent of YFP fluorescence after 40 min of infusion. Another microelectrode was used to pass current pulses for basal stimulation (2 μA x 2 msec, every 33 sec) (Fig.1A, micropipette extending in from lower left) to evoke single action potentials, detected by intracellular voltage recording simultaneously from both pre- and post-synaptic sites (Fig 1A for sites of recording and Fig.1B middle and bottom traces). This protocol is referred to hereafter as "basal stimulation". Measurement of voltage changes at both pre- and postsynaptic sites allows for assessment of the efficiency of synaptic transmission. Strikingly, after 40 min of G85R-SOD1-YFP infusion, the postsynaptic action potential was no longer detected, with only a subthreshold PSP observable (Fig.1B, Vpost). By comparison, there was no change in the postsynaptic potential with a WT-SOD1-YFP infusion (Fig.1B Control) or with fluorescent dextran alone (Fig.1-1). A time course study of WT-SOD1-YFP and G85R-SOD1-YFP was carried out to observe the kinetic behavior of EPSPs from basal stimulation during the respective infusions (Fig.1C; note that points are shown only for every 10^{th} pulse, i.e. at 5 min intervals). With infusion of the mutant protein, the EPSP

slope began to reduce by ~10 min, and was completely lost by ~60-70 min. By contrast, no effect on EPSP was observed with WT-SOD1-YFP infusion for greater than 100 min (Fig.1C). Thus, in contrast with the absence of an observable effect of WT-SOD1 infusion upon postsynaptic EPSP, injection of monomeric G85R-SOD1-YFP produced a substantial time-dependent inhibition of synaptic transmission.

To rule out the possibility that synaptic defects were caused by physical damage induced by electrode impalement and microinjection, injection was stopped when postsynaptic action potentials were abolished. This allowed the diffusion of G85R-SOD1-YFP away from the synaptic terminal through the presynaptic axon. The EPSP slope started to increase 90min later as the presynaptic fluorescent intensity of G85R-SOD1-YFP significantly decreased and EPSPs were fully restored in about 2.5 hours after most mutant SOD1 had diffused out of the terminal (Fig.1-2). Normal synaptic transmission continued for more than 1 hour until a second injection of G85R-SOD1-YFP significantly inhibited synaptic transmission in the same fashion as the first injection. These results suggested that G85R-SOD1-YFP inhibits synaptic transmission at least in part by directly affecting neurotransmitter release from the synaptic terminal and this effect was reversible upon the removal of G85R-SOD1-YFP from the synaptic terminal.

G85R-SOD1-YFP impairs synaptic vesicle availability at the active zone

To examine whether G85R-SOD1-YFP inhibited synaptic transmission by affecting synaptic vesicle pool dynamics, we microinjected G85R-SOD1YFP or WT-SOD1-YFP for 15 min and then applied trains of high frequency stimulation (HFS) presynaptically (50 Hz for 5 sec, with 5 sec intervals between trains) and measured postsynaptic depression of EPSPs, which are proportional to the underlying EPSCs and are uncontaminated by action potentials, to determine the size of the readily releasable pool (RRP) and the rate of vesicle mobilization from the reserved pool (RP). EPSP slopes during both the 1st train of a series trains of HFS (Fig.2A) and the 6th train (Fig.2-1) were compared in WT and G85R synapses. For controls, there was a two-phase diminution of EPSP slope across the 250 spikes, whereas with G85R synapses the first phase was barely detectable during the 6th train of HFS and was significantly inhibited

during the 1st train. The first phase is generally associated with utilization of the RRP, which appears to be smaller with the mutant, whereas the second phase is generally associated with utilization of the RP, which appears to be present in both with significant reduction by G85R-SOD1-YFP. To further measure these pools, the EPSP slope values were continuously integrated across one train of the same synapse prior to infusion and one train after 30 min of WT- or G85R-SOD1-YFP infusion. The EPSPs of each condition were integrated and averaged to generate traces (Fig.2B). Notably, the WT-SOD1 trace resembled that of the preinfusion trace (not shown), indicating that WT-SOD1 has little effect on synaptic vesicle availability and mobilization, whereas G85R-SOD1 trace exhibited integrated values that were substantially lower than those of WT-SOD1. The relative size of the RRP was determined for each condition by intersection of slope with the Y axis, and the mobilization rate from the RP was directly determined from the slopes (dotted lines; linear fit of the integrated EPSP slopes from the last 50 time points). The values and statistics for independent experiments are shown (n=11 for WT and n=6 for G85R, Fig.2C). G85R-SOD1-YFP drastically reduced both the RRP size and the vesicle mobilization rate from RP to RRP as compared with WT-SOD1-YFP. Therefore, reduced RRP size and slower RP mobilization rate, could lead to the loss of synaptic transmission.

Electron microscopy (EM) of WT-SOD1-YFP and G85R-SOD1-YFP-infused synapses

To visualize the synaptic vesicles directly, we carried out EM analyses of synapses infused for 40 min under basal stimulation with the respective proteins (*n = 3* for each group). The WT-SOD1-YFP-infused synapses exhibited normal morphology with abundant packing of synaptic vesicles against the presynaptic membrane, comparable to published EM data (Augustine et al. 2006) of normal squid giant synapse (Fig.3A, red * indicates an active zone, AZ), whereas the G85R-SOD1-YFP-infused synapses reproducibly exhibited synaptic vesicles that did not abut the membrane at active zones, lying in a zone distant from it (Fig.3B). The vesicles present in this zone also appeared generally larger, less compact in morphology and reduced in number relative to WT-SOD1 synapses. We also consistently observed additional structures, e.g. in this image, what appears to be a pre-autophagosome (labeled by blue #) and two adjoining prelysosomes (labeled by purple ^). By contrast we did not observe such structures in WT-

SOD1-infused presynaptic active zones. Notably, many of the pre-autophagosomes appeared to contain vesicles. This potentially reflects a local mechanism to remove G85R-SOD1-YFP-affected synaptic vesicles in the RRP and a subpopulation of vesicles in the RP, whereas, interestingly, the most remote RP pools appear to be spared, suggesting a potential source for synaptic vesicle supply, which may help restoring synaptic function if released upon proper stimulations. More detailed characterization of affected vesicles was carried out by counting the number of electron lucent vesicles, clathrin coated vesicles, and large electron lucent vesicles per active zone as described previously (Morgan et al. 1999) (Fig.3C-F). Nested ANOVA analyses suggested that while clathrin coated vesicles did not seem to be affected by G85R-SOD1, the total number of available synaptic vesicles was dramatically reduced. A cumulative measurement of AZs (102 across 3 biological repeats per group) infused with WT-SOD1 or G85R-SOD1 (binned by 50μm in distance) showed that such reductions seem to be evenly distributed in the RRP regardless of the distance from the membrane (Fig.3G-I). Due to the limited number of vesicles further away from the AZs (>675μm) in both groups, the increase in the relative vesicle distribution in that vicinity didn't seem to be statistically different between the G85R-SOD1-infused synapses and the WT-SOD1-infused synapses. This is further confirmed by the cumulative vesicle distribution curves (without binning) in WT and G85R-SOD1 synapses (Fig.3I).

Prevention of G85R-SOD1-YFP-associated synaptic deficits by intermittent HFS (iHFS)

Unexpectedly, when a single train of high frequency stimulation (HFS; 50 Hz for 5 sec) was applied presynaptically every 30 min, G85R-SOD1-YFP-infused synapses, otherwise receiving continuous basal stimulation, maintained constant EPSPs for over 8 hr (Fig.4A-C). This contrasts with the finding (Fig.1) that in the setting of G85R-SOD1-YFP infusion, continuous basal stimulation leads to steady decline and then complete loss of EPSPs within 40-60 min. This also contrasts with the finding (Fig.2) that continuous HFS trains with 5sec intervals also inhibited synaptic transmission by depletion of the RRP. Correlating with maintenance of healthy physiology, synaptic vesicle dynamics appeared to be normal, as demonstrated by presence of the first phase of EPSP slope during a single 50 Hz train, reflecting presence of an RRP resembling wild-type (Fig.4D). Additionally, the integrated EPSP slope averaged across

multiple 50 Hz trains now resembled that of WT-SOD1-YFP synapses (n = 6 for each, Fig.4E). Finally, in EM analyses (Fig.4F), consistent with presence of a normal RRP, vesicles were observed abutting the active zone after iHFS was applied to a synapse infused with G85R-SOD1-YFP for 6 hours These results indicate that iHFS is able to preserve the RRP in the face of G85R-SOD1-YFP infusion. Interestingly, in G85R-SOD1-injected synapses *(3 out of 5)* with dramatic decreases in the slope of the PSP but remaining >50, application of one HFS train restored EPSP slope and the RRP size, without rescuing vesicle mobilization rate (Fig.4-1). However, in the other 2 synapses where PSP slopes dropped to below 50, adding one HFS further reduced them to almost 0. This suggests that to achieve the rescuing effects, the timing of the HFS application with regard to existing synaptic strength is important. However, the underlying molecular mechanism of this rescuing effect is unclear and requires further study. Altogether, the intermittent stimulation reverses toxicity of the misfolded protein by restoring synaptic vesicle availability at the active zone.

G85R-SOD1 induces Ca^{2+} increase in the presynaptic terminal

Intrigued by the rescuing effect of iHFS in G85R-SOD1-infused synapses, we examined potential mechanisms. Since iHFS is known to alter Ca^{2+} dynamics, we wondered if aberrant Ca^{2+} signaling may underlie G85R-SOD1-YFP toxicity. To test this possibility, we performed ratiometric Ca^{2+} imaging using Fura-2, a fluorescent Ca^{2+} indicator dye, which was delivered to the presynaptic axon electrophoretically and allowed to diffuse into the "palm" and presynaptic branches (Fig.5A, regions of interest (ROIs) were selected to show 1: "palm", 2-6: presynaptic axon which forms the giant synapse, and 7: another small presynaptic branch). In parallel, the presynaptic axon was subjected to basal stimulation while both pre- and post-synaptic membrane potentials were recorded. The presence of Fura-2 provides an indication of changes in Ca^{2+} levels and location during stimulation. To avoid interference with Ca^{2+} imaging, WT-SOD1 and G85R-SOD1 constructs used in these studies lacked the YFP tag and injections were monitored by co-perfusion of Tetramethylrhodamine-dextran. While overall characteristics of synaptic function are similar with the introduction of Fura-2, the impairment of synaptic transmission by G85R-

SOD1 was delayed in the presence of Fura-2 (>60 min vs. previously less than 30 min after G85R-SOD1 injection), probably due to the buffering of Ca^{2+} by indicator dye. This impairment was correlated with a concurrent rise in Ca^{2+} levels at 60 min. Synapses injected with Fura-2 alone or Tetramethylrhodamine-Dextran alone kept constant EPSP normally for >2hr as those injected with WT. Furthermore, synapses injected with WT-SOD1 behaved similarly as those with WT-SOD1-YFP, excluding the potential role of YFP tag on synaptic transmission.

G85R-SOD1 infusion (*n = 19*) caused increases of Ca^{2+} throughout the presynaptic terminal compared with WT controls (*n = 12*), as derived from the ratios of (fluorescent intensity^{360nm})/(fluorescent intensity^{390nm}) averaged across ROIs 2-6 (Fig.5B). While WT-SOD1 under basal stimulation showed no change in Ca^{2+} concentration after 1hr protein infusion (Fig.5C), G85R-SOD1 increased global Ca^{2+} concentration in the "palm", the presynaptic giant axon (PreG), as well the other small presynaptic branch (PreS), with the most significant elevation at the site of G85R-SOD1 injection (Fig.5D) perhaps due to the highest G85R-SOD1 concentration on the injection site. Both the "palm" and PreS regions, further away from the injection site, would contain lower concentrations of mutant protein due to diffusion. Interestingly, the "palm" which lacks plasma membrane Ca^{2+} channels and doesn't normally show Ca^{2+} increases during HFS did not exhibit increased Ca^{2+} with WT-SOD1 (Fig.5-1A), consistent with earlier findings (Smith et al. 1993). However, in the presence of G85R-SOD1, the "palm" also displayed aberrant Ca^{2+} increases with HFS (Fig.5-1B), suggesting that sources of Ca^{2+} other than plasma membrane Ca^{2+} channels may contribute to this Ca^{2+} misregulation. Taken together, the evidence suggests that G85R-SOD1-induced Ca^{2+} influx may mediate its inhibitory effects on synaptic transmission and the effect may depend upon intracellular Ca^{2+} stores.

Given that iHFS rescued G85R-SOD1-associated synaptic defects, we wondered if iHFS could correct the aberrant localization of Ca^{2+} increases. Fura-2 ratiometric Ca^{2+} imaging demonstrated Ca^{2+} increases during HFS in both WT- and G85R-SOD1-injected synapses (Fig.5-1), confirming previous findings of HFS on Ca^{2+} dynamics by others (Smith et al. 1993). In the presence of G85R-SOD1, Ca^{2+}

concentrations in the "palm" appeared more variable across the synapses, with some "palm" regions showing Ca^{2+} increases as high as those in the synaptic terminal, suggesting high baseline Ca^{2+} concentration. However, there seemed to be no significant difference between WT-SOD1 (n = 12) and G85R-SOD1 (n = 19) injected synapses at the injection site and the other locations within the presynaptic terminals during iHFS, indicating normal Ca^{2+} channel functions at the injection site, thereby excluding the possibility of physical membrane damage caused by the injection. Consistent with iHFS-rescue in synaptic physiology and in contrast to G85R-SOD1-induced Ca^{2+} influx in the absence of iHFS, aberrant Ca^{2+} activation was not observed after iHFS in G85R-SOD1-injected synapses (Fig.5E and F). These results suggest that iHFS may reset Ca^{2+} dynamics in the terminal and prevent the local Ca^{2+} overloads that contribute to synaptic dysfunction induced by G85R-SOD1.

EGTA prevents toxic effects of G85R-SOD1-YFP on synaptic physiology and morphology

The iHFS-rescue experiments in combination with Ca^{2+} imaging and the delayed inhibition produced by Fura-2 suggested that aberrant Ca^{2+} activation by G85R-SOD1 may be the cause of synaptic inhibition. To further test this hypothesis, we chelated free Ca^{2+} in the presynaptic terminal by co-injecting 50mM EGTA (final concentration at 5-10mM in the synapse). Previous studies had shown that EGTA levels less than 80mM do not affect synaptic transmission (Adler et al. 1991). EGTA was sufficient to block the inhibitory effects of G85R-SOD1-YFP on synaptic transmission and G85R-SOD1-YFP-injected synapses maintained steady EPSPs for over 2 hours without iHFS (n = 6), which was comparable to WT-SOD1-YFP-injected synapses (Fig.6A and Fig. 6-1, 5 WT-SOD1- and 8 G85R-SOD1-infused synapses were also shown in Fig.1C). Not surprisingly, ratiometric Ca^{2+} imaging using Fura-2 did not show any local Ca^{2+} increases in synapses co-injected with G85R-SOD1 and EGTA (Fig.6B and C). Defects in synaptic vesicle pools, number and distribution induced by G85R-SOD1 were also corrected by EGTA, as evidenced by the usual RRP size, and normal mobilization rate (Fig.6D-E). Furthermore, EM showed comparable numbers of synaptic vesicles at the active zones (Fig.6F). The numbers of docked and electron lucent synaptic vesicles were similar between the WT-SOD1 and G85R-SOD1+EGTA-infused

synapses, while EGTA might slightly increase clathrin coating (Fig.6G, *102* synapses for each group). These results suggest that Ca^{2+} dysregulation may underlie G85R-SOD1-associated synaptic dysfunctions and that limiting increases in free cytoplasmic Ca^{2+} with EGTA may restore normal synaptic morphology and function.

DISCUSSION

The discovery of giant fibers in the squid nervous system by J.Z. Young (Young and Keynes 2005) more than 80 years ago led to several milestone discoveries in modern neuroscience, including the Nobel-prize-winning work on ionic mechanisms for initiating and propagating action potentials by Andrew Huxley and Alan Hodgkin (Schwiening 2012). Although advanced imaging and genetic tools as well as new model systems have been developed in recent years, these classical mature synapse and axon models continue to be utilized to understand fundamental neurobiology and provide a unique model to study molecular mechanisms of human neurological diseases. For example, the original discovery of the molecular motor kinesin in isolated axoplasm from the squid led to studies of axonal trafficking deficits resulting from altered motor function in several neurodegenerative diseases (Song et al. 2016; Brady and Morfini 2017). In a similar way, studies of molecular mechanisms underlying basic synaptic physiology in the squid giant synapse have led to exploration of disease mechanisms involving synaptic dysfunction (Moreno et al. 2009). Here, we use the giant axo-axonic synapse in the squid stellate ganglion to study synaptic actions of mutant human SOD1 (G85R-SOD1) protein, which causes a familial form of Amyotrophic Lateral Sclerosis.

Presynaptic injection of G85R SOD1 inhibits neurotransmission by disturbing synaptic vesicle physiology

Synaptic loss at affected neuromuscular junctions leading to a dying-back neuropathy appears to be a primary defect associated with pathology in ALS patients and mouse models bearing G85R-SOD1 mutations. Consistent with these observations, we found that infusion of ALS-associated human G85R mutant SOD1 protein but not the wild-type SOD1 into the presynaptic terminal of the squid giant synapse

(SGS) significantly inhibited EPSPs, leading to a failure in eliciting postsynaptic action potentials. This occurred within 30min of continuous infusion into the presynaptic terminal without diminishing the presynaptic action potentials, while infusion of the WT-SOD1 had no effect on synaptic transmission as evidenced by sustained firing of synapses with constant EPSPs (Fig.1).

High frequency stimulus protocols designed to deplete the readily releasable pool (RRP) of presynaptic vesicles showed that vesicle dynamics were significantly inhibited by G85R-SOD1, reducing both the size of the RRP and the mobilization rate from the reserved pool (RP) to the RRP (Fig.2). This finding was further validated by EM data that demonstrated significant reductions of synaptic vesicles at active zones in the presence of G85R-SOD1 protein (Fig.3). Ultrastructural studies provided additional evidence of altered vesicle trafficking as membranous structures resembling multivesicular bodies and autophagosomes were identified in presynaptic regions infused with G85R-SOD1, but not WT-SOD1. Inhibition of synaptic transmission was reversed by stopping presynaptic infusion of G85R-SOD1 and allowing sufficient time for the protein to diffuse out of the synapse *via* the presynaptic giant axon (Fig.1-2), which suggested that the synaptic machinery was not physically and permanently damaged.

Nature of synaptic vesicle disturbance

A clue to the mechanism for G85R-SOD1-induced synaptic inhibition came from an experiment where the synapse was exposed to intermittent HFS (iHFS) at 30min intervals before and during G85R-SOD1 infusion. This was expected to inhibit synaptic transmission based on earlier results showing that continuous HFS depleted presynaptic RRP. Unexpectedly, G85R-SOD1-synapses exposed to iHFS maintained constant EPSPs for over 7 hours, exhibiting normal synaptic vesicle dynamics and normal numbers of synaptic vesicles at active zones despite the presence of pathogenic SOD1 protein (Fig.4). This finding led us to examine Ca^{2+} dynamics as HFS is known to redistribute Ca^{2+} both temporally and spatially (Smith et al. 1993).

Live cell ratiometric Ca^{2+} imaging studies showed that G85R-SOD1 consistently increased Ca^{2+} levels in presynaptic terminals with the largest increases at the injection site, the site with highest G85R-SOD1 concentration. Surprisingly, Ca^{2+} levels were also increased in the “palm” region, which lacks

plasmalemmal Ca^{2+} channels and normally does not exhibit Ca^{2+} increases in response to HFS (Fig.5). These data suggested that the source of Ca^{2+} may not be restricted to or dependent on local plasma membrane Ca^{2+} channels. This agrees with previous findings that Ca^{2+} influx solely through voltage-gated Ca^{2+} channels is not able to induce motor neuron death (Van den Bosch et al. 2002). Instead, release of Ca^{2+} from endoplasmic reticulum and/or mitochondrial stores is required, and these organelles may release Ca^{2+} in response to misfolded G85R-SOD1 protein.

Co-injection of EGTA and application of iHFS prevent physiopathology

If increased free Ca^{2+} levels are responsible for synaptic failure, co-injection of EGTA, a Ca^{2+} chelator, at levels that do not affect synaptic transmission at the squid giant synapse should prevent synaptic inhibition by G85R-SOD1 by buffering free Ca^{2+}. Consistent with the conclusion that presynaptic increases in free Ca^{2+} levels were responsible for the observed synaptic dysfunction, EGTA prevented inhibition of synaptic transmission when co-injected into the presynaptic terminal with G85R-SOD1, as documented by 1) EPSPs remained constant for over 2 hours; 2) sufficient numbers of synaptic vesicle were present at the active zones with normal mobilization from RP to RRP; and 3) cytoplasmic free Ca^{2+} levels did not increase (Fig.6). Similar effects were also achieved by iHFS applied every 30min for over 7 hours (Fig.4). Interestingly, iHFS also abolished the Ca^{2+} increases induced by G85R-SOD1 (Fig.5) perhaps by redistributing Ca^{2+} and restoring homeostasis. This process may alter regulation of other organelles such as ER, mitochondria, and autophagosomes in the synapse to restore overall synaptic health. However, determining the exact molecular mechanisms requires more in-depth studies.

Questions remain as to how increased cytoplasmic free Ca^{2+} alters synaptic vesicle dynamics in the presynaptic terminal. Ca^{2+} is a key player in many cellular and subcellular processes, is required for regular synaptic function, and is normally tightly regulated. In normal synapses, free Ca^{2+} increases are largely restricted to the active zone through local plasmalemmal channels during synaptic transmission (Sudhof 2004). The levels of EGTA used in these studies do not affect Ca^{2+} influx at active zones but do buffer cytoplasmic free Ca^{2+}. There are multiple Ca^{2+} sensors with a wide range of affinities in the presynaptic compartment, all of which may contribute to one or more of the complex steps involved in

synaptic transmission and synaptic vesicle dynamics. While the role of some of these sensors is established, such as evidence that synaptotagmin is the Ca^{2+} sensor for synaptic vesicle fusion and neurotransmitter fast release, the physiological roles for many others remain unclear (Sudhof 2004).

The existing literature has suggested a variety of potential mechanisms for Ca^{2+} related pathology in both human and mouse ALS-vulnerable neurons (Grosskreutz, Van Den Bosch, and Keller 2010), such as the subgroups of motor neurons in spinal cord and brainstem expressing low levels of Ca^{2+} buffering proteins, even at the presymptomatic stages. Similarly, Ca^{2+} dysregulation has also been observed in several other neurodegenerative diseases and may lead to Unfolded Protein Responses (UPR) and ER-stress-related signaling activation (Remondelli and Renna 2017; Walker and Atkin 2011; Hetz and Saxena 2017; Grosskreutz, Van Den Bosch, and Keller 2010), Ca^{2+} permeable AMPA receptor dysregulation (Tortarolo et al. 2006; Tateno et al. 2004; Van Den Bosch et al. 2006), ER/mitochondria membrane collapse (Watanabe et al. 2016; Bernard-Marissal, Chrast, and Schneider 2018; Tortarolo et al. 2006), and aberrant Ca^{2+} influx in affected neurons and glia. In addition, changes in protein expression in affected motor neurons (e.g. Ca^{2+} channels and regulators) may also contribute to dysregulation of Ca^{2+} levels in disease. While altered transcription may play a role in the slow progression of the disease, this is unlikely to contribute here given the time scale and reversibility of these effects as well as the lack of strong evidence of local transcription in the squid giant synapse.

In conclusion, our results in the SGS indicate that mutant SOD1 affects the regulation of free Ca^{2+} levels in the presynaptic terminal, leading to a disruption of normal vesicle trafficking. These effects were not restricted to regions near the active zones but were more extensive and affected regions of the presynaptic compartment that lack plasmalemmal Ca^{2+} channels. The effects of mutant SOD1 may occur without affecting the activity of local plasmalemmal Ca^{2+} channels required for neurotransmitter release at the active zone, given that 1) presynaptic regions lacking Ca^{2+} channels also showed increased levels of free Ca^{2+}, 2) low levels of EGTA can reduce free Ca^{2+} levels in the presence of G85R-SOD1 without affecting Ca^{2+} influx through plasmalemmal Ca^{2+} channels responsible for normal synaptic transmission, and 3) the discovery that iHFS could rescue synaptic transmission. The effect of iHFS was unexpected

and further argues for normal function of active zone Ca^{2+} channels in the plasmalemma independent of intracellular stores of Ca^{2+}. The effect of iHFS suggests that further study is needed of how patterns of activity can preserve synaptic function and this may be a basis for novel therapeutic interventions in ALS.

The effects observed here may relate to those observed earlier in the squid giant axon innervating muscles in the mantle. There we found that G85R-SOD1-YFP inhibited axonal trafficking of presynaptic vesicles by activating a MAPK stress pathway, which impaired kinesin-based transport responsible for anterograde cargo transport (Song et al. 2013). In addition, we observed that that G85R-SOD1 was associated with several synaptic proteins critical for synaptic transmission, such as Synapsin and Syntaxin-binding protein 5, at a much higher level than WT-SOD1-YFP. HSP110, an HSC70 Co-Chaperone which prevented the neurotoxicity of G85R-SOD1 in the axon by potentially sequestering or refolding G85R-SOD1, also abolished the association of Synapse-associated protein and Syntaxin-binding protein 5 with G85R-SOD1-YFP (Song et al. 2013). The roles that G85R-SOD1 interactions with synaptic proteins may play in affecting synaptic vesicle dynamics as well as regulation of these interactions *via* Ca^{2+} dependent or independent pathways remain to be determined. Various neuropathogenic changes have been proposed to be a consequence of Ca^{2+} dysregulation, such as UPR and autophagy, in ALS and several other neurodegenerative diseases. Our EM data (Fig.6) showed that EGTA, when co-injected with G85R-SDO1, restored synaptic morphology and prevented the formation of pre-autophagosome and adjoining pre-lysosomes, which were observed when presynaptic G85R-SOD1 was injected alone.

Implication of acute toxic effects of G85R-SOD1 on squid giant synapse physiology as relates to longer term ALS pathology in mammalian synapses

Like many other adult-onset neurodegenerative diseases, one big puzzle in the field is “why does it take 40-50 years to develop ALS?”. Several disease-related processes occur during aging which can be overcome in young neurons due to robust compensatory mechanisms. In this study, we focus on acute effects of pathogenic SOD1, but a number of age-related factors may explain the delayed onset of clinical symptoms.

512 Unlike the acute injection of pathogenic SOD1 in this study where we observed the presence of pre-
513 autophagosome and pre-lysosome formation within the time frame of both electrophysiological
514 recordings and morphological studies, ALS-associated mutant SOD1 in patients misfolds and
515 accumulates gradually to pathological levels over time, allowing adaptive changes in cellular and
516 molecular mechanisms underlying synaptic transmission. This is due to, at least partially, mechanisms for
517 actively removing pathogenic proteins in early stages of disease, which may be sufficient to slow the
518 accumulation of toxic materials. However, these clearance mechanisms may eventually be unable to keep
519 up with misfolded protein accumulations. By directly injecting defined levels of mutant SOD1 into an
520 isolated squid giant synapse system, we ensured accumulation of misfolded protein locally in the
521 synapses within a short period of time which limits compensatory effects in the isolated synapse with
522 little protein degradation and synthesis in this time frame.
523 Similar to robust protein homeostatic pathways during development and maturation, Ca^{2+} buffering
524 mechanisms and synaptic transmission may be redundant early on in the complex system such as the
525 mammalian models where neuronal circuits (including the other cell types) are intact and dynamic. They
526 can adapt to slowly increased stresses created by the presence of mutant SOD1, much as synaptic
527 functions exhibit adaptive changes during normal aging. The use of isolated acute preparations of giant
528 synapse also eliminates the possibility that transcriptional changes of synaptic proteins can compensate
529 for the effects of toxic proteins on synaptic transmission machinery. For example, the question of
530 whether ALS-affected neurons show hyper- or hypo- excitability has been debated for some time. As a
531 matter of fact, several groups have reported hyperexcitability of motor neurons at early stages followed by
532 hypoexcitability at later stages of ALS in both iPSC culture models and in mouse models. These changes
533 may be due to various compensatory mechanisms at the molecular, cellular and systemic levels which
534 also may contribute to the delayed onset of symptoms. Here, we can isolate inhibitory effects due to the
535 simplicity of the squid synapse model system where many other factors, such as compensation from other
536 neurons, changes in gene expression or axonal transport, or the impact of a complex environment can no
537 longer play a role.

Furthermore, it is worth keeping in mind that synaptic loss, as a result of gradual decrease in synaptic strength as demonstrated here, occurs long before cell death and can be observed in presymptomatic stages of both ALS mice and patients. By measuring EPSP slopes and vesicle dynamics in the squid giant synapse, we have provided a sensitive readout of neurotransmission in real time and revealed changes in synaptic strength which are more subtle in pre-symptomatic patients and mouse models but are detectable long before clinically relevant behavioral abnormalities appear. Correlating Ca^{2+} dynamics and HFS effects with synaptic health in real time illuminates the kinetic changes in the presynaptic terminal with high temporal and spatial resolution, which suggests the importance of identifying potential therapeutic time windows. The acute effects demonstrated here may illustrate molecular mechanisms underlying disease pathology that are manifested over time in patients.

Relevant to mammalian physiology and pathology, the squid giant synapse also shares fundamental synaptic machineries with neuromuscular junctions in human, making it a unique ALS-disease model with a potential for answering important but otherwise difficult questions about pathogenic mechanisms and synaptic transmission in motor neuron diseases. The squid giant synapse provides a unique platform for 1) performing live measurements of both pre- and post- synaptic activities in response to disease-associated proteins with temporal and spatial resolutions surpassing those in most other model systems; 2) conducting morphological studies in the same preparations characterized by live-imaging of cellular and molecular pathways, electrophysiological studies and electron microscopy in the same sample; 3) evaluating pharmacological inhibitors, biochemical tools, and electrophysiological protocols that may rescue disease phenotypes in a time dependent manner; and 4) identifying translatable mechanistic findings, due to the highly conserved synaptic machinery, that will provide better understanding and treatment of multiple neurodegenerative diseases where misfolded proteins cause disease pathology.

In conclusion, the development of novel models for study of neurodegenerative diseases such as those using the squid nervous system has the potential to provide unique insights into disease mechanisms. For example, the combination of our electrophysiological studies in the giant synapse with studies of axonal transport in isolated axoplasm from the postsynaptic giant axon of the squid, allowed us

to identify signaling pathways altered by these pathogenic proteins (Song et al. 2013). These results were then developed further in mouse models of ALS and patient tissues or iPSCs. Our results here are also consistent with previous findings of Ca^{2+} dysregulation and synaptic dysfunction in both ALS mice and patient derived neurons (Tradewell et al. 2011; Grosskreutz, Van Den Bosch, and Keller 2010; Leal and Gomes 2015). For example, affected neurons exhibit aberrant Ca^{2+} dynamics, which leads to hyperexcitability or hypoexcitability at various stages (Wainger et al. 2014; Devlin et al. 2015; Martinez-Silva et al. 2018). Further, oculomotor neurons, which are relatively spared in ALS, have a higher buffering capacity for Ca^{2+} (Vanselow and Keller 2000; Obal, Engelhardt, and Siklos 2006), which was thought to contribute to their overall resistance to pathology in patients and mouse models. Those data were unclear, however, as to whether these changes involved plasmalemmal Ca^{2+} channels or intracellular Ca^{2+} stores or both, an issue that could be addressed in the SGS.

Given recent work on the squid genome and improved mariculture protocols that have the potential to allow systematic long-term studies of squid nervous systems, there will be opportunities to develop novel transgenic ALS squid models. Therefore, studies using the squid giant synapse will continue to complement studies using human iPSCs and animal models of ALS as we seek to understand how multiple disease related pathways can independently affect the pleiotropic neuronal functions that interact to produce the phenotype of ALS, a multifactorial disease with a complex disease pathology.

590

591

592

593 **REFERENCE:**

594 Adler, E. M., G. J. Augustine, S. N. Duffy, and M. P. Charlton. 1991. 'Alien intracellular calcium chelators
595 attenuate neurotransmitter release at the squid giant synapse', *J Neurosci*, 11: 1496-507.
596 Augustine, G. J. 1990. 'Regulation of transmitter release at the squid giant synapse by presynaptic
597 delayed rectifier potassium current', *J Physiol*, 431: 343-64.
598 Augustine, G. J., and M. P. Charlton. 1986. 'Calcium dependence of presynaptic calcium current and
599 post-synaptic response at the squid giant synapse', *J Physiol*, 381: 619-40.
600 Augustine, G. J., M. P. Charlton, and R. Horn. 1988. 'Role of calcium-activated potassium channels in
601 transmitter release at the squid giant synapse', *J Physiol*, 398: 149-64.
602 Augustine, G. J., J. R. Morgan, C. A. Villalba-Galea, S. Jin, K. Prasad, and E. M. Lafer. 2006. 'Clathrin and
603 synaptic vesicle endocytosis: studies at the squid giant synapse', *Biochem Soc Trans*, 34: 68-72.
604 Bernard-Marissal, N., R. Chrast, and B. L. Schneider. 2018. 'Endoplasmic reticulum and mitochondria in
605 diseases of motor and sensory neurons: a broken relationship?', *Cell Death Dis*, 9: 333.
606 Bloedel, J., P. W. Gage, R. Llinas, and D. M. Quastel. 1966. 'Transmitter release at the squid giant synapse
607 in the presence of tetrodotoxin', *Nature*, 212: 49-50.
608 Brady, S. T., and G. A. Morfini. 2017. 'Regulation of motor proteins, axonal transport deficits and adult-
609 onset neurodegenerative diseases', *Neurobiol Dis*, 105: 273-82.
610 Bruijn, L. I., M. K. Houseweart, S. Kato, K. L. Anderson, S. D. Anderson, E. Ohama, A. G. Reaume, R. W.
611 Scott, and D. W. Cleveland. 1998. 'Aggregation and motor neuron toxicity of an ALS-linked SOD1 mutant
612 independent from wild-type SOD1', *Science*, 281: 1851-4.
613 Bunton-Stasyshyn, R. K., R. A. Saccon, P. Fratta, and E. M. Fisher. 2015. 'SOD1 Function and Its
614 Implications for Amyotrophic Lateral Sclerosis Pathology: New and Renascent Themes', *Neuroscientist*,
615 21: 519-29.
616 Devlin, A. C., K. Burr, S. Borooah, J. D. Foster, E. M. Cleary, I. Geti, L. Vallier, C. E. Shaw, S. Chandran, and
617 G. B. Miles. 2015. 'Human iPSC-derived motoneurons harbouring TARDBP or C9ORF72 ALS mutations are
618 dysfunctional despite maintaining viability', *Nat Commun*, 6: 5999.
619 Fischer, L. R., D. G. Culver, P. Tennant, A. A. Davis, M. Wang, A. Castellano-Sanchez, J. Khan, M. A. Polak,
620 and J. D. Glass. 2004. 'Amyotrophic lateral sclerosis is a distal axonopathy: evidence in mice and man',
621 *Exp Neurol*, 185: 232-40.
622 Frey, D., C. Schneider, L. Xu, J. Borg, W. Spooren, and P. Caroni. 2000. 'Early and selective loss of
623 neuromuscular synapse subtypes with low sprouting competence in motoneuron diseases', *J Neurosci*,
624 20: 2534-42.
625 Fukuda, M., J. E. Moreira, F. M. Lewis, M. Sugimori, M. Niinobe, K. Mikoshiba, and R. Llinas. 1995. 'Role
626 of the C2B domain of synaptotagmin in vesicular release and recycling as determined by specific
627 antibody injection into the squid giant synapse preterminal', *Proc Natl Acad Sci U S A*, 92: 10708-12.
628 Ghasemi, M., and R. H. Brown, Jr. 2018. 'Genetics of Amyotrophic Lateral Sclerosis', *Cold Spring Harb
629 Perspect Med*, 8.
630 Grosskreutz, J., L. Van Den Bosch, and B. U. Keller. 2010. 'Calcium dysregulation in amyotrophic lateral
631 sclerosis', *Cell Calcium*, 47: 165-74.
632 Hegedus, J., C. T. Putman, and T. Gordon. 2007. 'Time course of preferential motor unit loss in the SOD1
633 G93A mouse model of amyotrophic lateral sclerosis', *Neurobiol Dis*, 28: 154-64.

Hetz, C., and S. Saxena. 2017. 'ER stress and the unfolded protein response in neurodegeneration', *Nat Rev Neurol*, 13: 477-91.

Katz, B., and R. Miledi. 1967. 'A study of synaptic transmission in the absence of nerve impulses', *J Physiol*, 192: 407-36.

———. 1977. 'Suppression of transmitter release at the neuromuscular junction', *Proc R Soc Lond B Biol Sci*, 196: 465-9.

Leal, S. S., and C. M. Gomes. 2015. 'Calcium dysregulation links ALS defective proteins and motor neuron selective vulnerability', *Front Cell Neurosci*, 9: 225.

Lin, J. W., M. Sugimori, R. R. Llinas, T. L. McGuinness, and P. Greengard. 1990. 'Effects of synapsin I and calcium/calmodulin-dependent protein kinase II on spontaneous neurotransmitter release in the squid giant synapse', *Proc Natl Acad Sci U S A*, 87: 8257-61.

Llinas, R., T. L. McGuinness, C. S. Leonard, M. Sugimori, and P. Greengard. 1985. 'Intraterminal injection of synapsin I or calcium/calmodulin-dependent protein kinase II alters neurotransmitter release at the squid giant synapse', *Proc Natl Acad Sci U S A*, 82: 3035-9.

Llinas, R. R., M. Sugimori, and R. B. Silver. 1994. 'Localization of calcium concentration microdomains at the active zone in the squid giant synapse', *Adv Second Messenger Phosphoprotein Res*, 29: 133-7.

Llinas, R., I. Z. Steinberg, and K. Walton. 1980. 'Transmission in the squid giant synapse: a model based on voltage clamp studies', *J Physiol (Paris)*, 76: 413-8.

———. 1981. 'Presynaptic calcium currents in squid giant synapse', *Biophys J*, 33: 289-321.

Martinez-Silva, M. L., R. D. Imhoff-Manuel, A. Sharma, C. J. Heckman, N. A. Shneider, F. Roselli, D. Zytnicki, and M. Manuel. 2018. 'Hypoexcitability precedes denervation in the large fast-contracting motor units in two unrelated mouse models of ALS', *Elife*, 7.

Moloney, E. B., F. de Winter, and J. Verhaagen. 2014. 'ALS as a distal axonopathy: molecular mechanisms affecting neuromuscular junction stability in the presymptomatic stages of the disease', *Front Neurosci*, 8: 252.

Moreno, H., E. Yu, G. Pigino, A. I. Hernandez, N. Kim, J. E. Moreira, M. Sugimori, and R. R. Llinas. 2009. 'Synaptic transmission block by presynaptic injection of oligomeric amyloid beta', *Proc Natl Acad Sci U S A*, 106: 5901-6.

Morgan, J. R., X. Zhao, M. Womack, K. Prasad, G. J. Augustine, and E. M. Lafer. 1999. 'A role for the clathrin assembly domain of AP180 in synaptic vesicle endocytosis', *J Neurosci*, 19: 10201-12.

Obal, I., J. I. Engelhardt, and L. Siklos. 2006. 'Axotomy induces contrasting changes in calcium and calcium-binding proteins in oculomotor and hypoglossal nuclei of Balb/c mice', *J Comp Neurol*, 499: 17-32.

Pasinelli, P., M. E. Belford, N. Lennon, B. J. Bacskai, B. T. Hyman, D. Trotti, and R. H. Brown, Jr. 2004. 'Amyotrophic lateral sclerosis-associated SOD1 mutant proteins bind and aggregate with Bcl-2 in spinal cord mitochondria', *Neuron*, 43: 19-30.

Remondelli, P., and M. Renna. 2017. 'The Endoplasmic Reticulum Unfolded Protein Response in Neurodegenerative Disorders and Its Potential Therapeutic Significance', *Front Mol Neurosci*, 10: 187.

Sakowski, S. A., J. S. Lunn, A. S. Busta, S. S. Oh, G. Zamora-Berridi, M. Palmer, A. A. Rosenberg, S. G. Philip, J. J. Dowling, and E. L. Feldman. 2012. 'Neuromuscular effects of G93A-SOD1 expression in zebrafish', *Mol Neurodegener*, 7: 44.

Schwiening, C. J. 2012. 'A brief historical perspective: Hodgkin and Huxley', *J Physiol*, 590: 2571-5.

Smith, S. J., J. Buchanan, L. R. Osses, M. P. Charlton, and G. J. Augustine. 1993. 'The spatial distribution of calcium signals in squid presynaptic terminals', *J Physiol*, 472: 573-93.

Song, Y., M. Kang, G. Morfini, and S. T. Brady. 2016. 'Fast axonal transport in isolated axoplasm from the squid giant axon', *Methods Cell Biol*, 131: 331-48.

Song, Y., M. Nagy, W. Ni, N. K. Tyagi, W. A. Fenton, F. Lopez-Giraldez, J. D. Overton, A. L. Horwich, and S. T. Brady. 2013. 'Molecular chaperone Hsp110 rescues a vesicle transport defect produced by an ALS-associated mutant SOD1 protein in squid axoplasm', *Proc Natl Acad Sci U S A*, 110: 5428-33.
Sudhof, T. C. 2004. 'The synaptic vesicle cycle', *Annu Rev Neurosci*, 27: 509-47.
Sugimori, M., C. K. Tong, M. Fukuda, J. E. Moreira, T. Kojima, K. Mikoshiba, and R. Llinas. 1998. 'Presynaptic injection of syntaxin-specific antibodies blocks transmission in the squid giant synapse', *Neuroscience*, 86: 39-51.
Tateno, M., H. Sadakata, M. Tanaka, S. Itohara, R. M. Shin, M. Miura, M. Masuda, T. Aosaki, M. Urushitani, H. Misawa, and R. Takahashi. 2004. 'Calcium-permeable AMPA receptors promote misfolding of mutant SOD1 protein and development of amyotrophic lateral sclerosis in a transgenic mouse model', *Hum Mol Genet*, 13: 2183-96.
Taylor, J. P., R. H. Brown, Jr., and D. W. Cleveland. 2016. 'Decoding ALS: from genes to mechanism', *Nature*, 539: 197-206.
Tortarolo, M., G. Grignaschi, N. Calvaresi, E. Zennaro, G. Spaltro, M. Colovic, C. Fracasso, G. Guiso, B. Elger, H. Schneider, B. Seilheimer, S. Caccia, and C. Bendotti. 2006. 'Glutamate AMPA receptors change in motor neurons of SOD1G93A transgenic mice and their inhibition by a noncompetitive antagonist ameliorates the progression of amytrophic lateral sclerosis-like disease', *J Neurosci Res*, 83: 134-46.
Tradewell, M. L., L. A. Cooper, S. Minotti, and H. D. Durham. 2011. 'Calcium dysregulation, mitochondrial pathology and protein aggregation in a culture model of amyotrophic lateral sclerosis: mechanistic relationship and differential sensitivity to intervention', *Neurobiol Dis*, 42: 265-75.
Urushitani, M., A. Sik, T. Sakurai, N. Nukina, R. Takahashi, and J. P. Julien. 2006. 'Chromogranin-mediated secretion of mutant superoxide dismutase proteins linked to amyotrophic lateral sclerosis', *Nat Neurosci*, 9: 108-18.
Van Den Bosch, L., P. Van Damme, E. Bogaert, and W. Robberecht. 2006. 'The role of excitotoxicity in the pathogenesis of amyotrophic lateral sclerosis', *Biochim Biophys Acta*, 1762: 1068-82.
Van den Bosch, L., P. Van Damme, V. Vleminckx, E. Van Houtte, G. Lemmens, L. Missiaen, G. Callewaert, and W. Robberecht. 2002. 'An alpha-mercaptoacrylic acid derivative (PD150606) inhibits selective motor neuron death via inhibition of kainate-induced Ca2+ influx and not via calpain inhibition', *Neuropharmacology*, 42: 706-13.
Vanselow, B. K., and B. U. Keller. 2000. 'Calcium dynamics and buffering in oculomotor neurones from mouse that are particularly resistant during amyotrophic lateral sclerosis (ALS)-related motoneurone disease', *J Physiol*, 525 Pt 2: 433-45.
Wainger, B. J., E. Kiskinis, C. Mellin, O. Wiskow, S. S. Han, J. Sandoe, N. P. Perez, L. A. Williams, S. Lee, G. Boulting, J. D. Berry, R. H. Brown, Jr., M. E. Cudkowicz, B. P. Bean, K. Eggan, and C. J. Woolf. 2014. 'Intrinsic membrane hyperexcitability of amyotrophic lateral sclerosis patient-derived motor neurons', *Cell Rep*, 7: 1-11.
Walker, A. K., and J. D. Atkin. 2011. 'Stress signaling from the endoplasmic reticulum: A central player in the pathogenesis of amyotrophic lateral sclerosis', *IUBMB Life*, 63: 754-63.
Wang, J., G. W. Farr, D. H. Hall, F. Li, K. Furtak, L. Dreier, and A. L. Horwich. 2009. 'An ALS-linked mutant SOD1 produces a locomotor defect associated with aggregation and synaptic dysfunction when expressed in neurons of Caenorhabditis elegans', *PLoS Genet*, 5: e1000350.
Wang, J., G. W. Farr, C. J. Zeiss, D. J. Rodriguez-Gil, J. H. Wilson, K. Furtak, D. T. Rutkowski, R. J. Kaufman, C. I. Ruse, J. R. Yates, 3rd, S. Perrin, M. B. Feany, and A. L. Horwich. 2009. 'Progressive aggregation despite chaperone associations of a mutant SOD1-YFP in transgenic mice that develop ALS', *Proc Natl Acad Sci U S A*, 106: 1392-7.
Watanabe, S., H. Ilieva, H. Tamada, H. Nomura, O. Komine, F. Endo, S. Jin, P. Mancias, H. Kiyama, and K. Yamanaka. 2016. 'Mitochondria-associated membrane collapse is a common pathomechanism in SIGMAR1- and SOD1-linked ALS', *EMBO Mol Med*, 8: 1421-37.

Young, J. Z., and R. Keynes. 2005. 'The Functioning of the Giant Nerve Fibres of the Squid. 1938 - J.Z. and the discovery of squid giant nerve fibres', *J Exp Biol*, 208: 179-80.

LEGENDS

Figure 1. Presynaptic infusion of G85R-SOD1-YFP inhibited synaptic transmission. (A) Diagram of experimental setup. Presynaptic 2nd order giant axon branch (black) and postsynaptic 3rd order giant axon (red) form the giant synapse in the stellate ganglion. Two electrodes were inserted in the presynaptic axon, one at the "palm" to deliver electronic stimulation at 0.03 Hz (each pulse is 2μA for 2ms) and the other in the presynaptic terminal for recording presynaptic potentials as well as injecting 50μM SOD1 proteins and reagents of interest at 0.1 Hz, each injection was 50 psi for 250 ms. The 3rd electrode was inserted in the postsynaptic axon to record postsynaptic potentials. (B) Under current clamping condition, G85R-SOD1-YFP injected synapses showed reductions in postsynaptic potential (V_{post}) within 30min and a failure to elicit a postsynaptic action potential in 40min, compared with the control before injection. (C) EPSP slopes of WT-SOD1-YFP injected-synapses (*n = 5*) and G85R-SOD1-YFP-injected synapses (*n = 8*) were normalized to the initial time point (-30min), 30min before the beginning of SOD1 injections. Averaged EPSP slopes were plotted with error bars showing standard error. The thick black bar indicates the duration of SOD1 infusion starting at time 0. G85R-SOD1-YFP consistently inhibited synaptic transmission as shown by reductions in the EPSP slope, while WT-SOD1-YFP infusions showed no effect on EPSPs. Control synapses infused with fluorescent dextran showed normal firing similar to the WT-SOD1-YFP infused synapses (Fig.1-1). Moreover, synaptic function gradually recovered in G85R-SOD1-YFP-infused synapses after protein infusion was stopped, excluding the possibility of physical damage of synaptic machinery due to injection (Fig.1-2).

Figure 2. Presynaptic infusion of G85R-SOD1-YFP altered synaptic vesicle dynamics. (A) Series of six continuous trains of High frequency stimulation (HFS, each train is 50 Hz for 5 seconds with 5

seconds between trains) was applied to the synapses infused with SOD1 proteins for 15min prior to HFS trains. WT-SOD1-GFP-injected synapses showed constant EPSP slope at the beginning of each train suggesting robust neurotransmission (>200, also see Fig.2-1 for the 6th train). However, G85R-SOD1-YFP-injected synapse started to show reductions in synaptic transmission, as evidenced by the dramatic decrease in EPSP slopes taken during the 1st train both at the beginning and at the steady state, suggesting severe depletion of synaptic vesicles from both the readily releasable pools and the reserved pools. This inhibition was more obvious in the 6th train (Fig.2-1) (B) EPSPs of the 1st train from WT-SOD1-YFP-injected synapses (black, $n = 11$) and from G85R-SOD1-YFP-injected synapses (red, $n = 6$) were integrated and averaged, followed by linear fit. The intersection with Y axis indicated the size of the readily releasable vesicle pool (RRP) and the slope indicated the mobilization rate of vesicles from the reserved pool (RP) to RRP. (C) Normalized to baseline values before the injection of SOD1-YFP, RRP size and mobilization rate from the 1st train were plotted as individual biological replicates ($n = 11$ for WT-SOD1-infused synapses and $n= 6$ for G85R-SOD1-infused synapses) to show significant reductions in both RRP and mobilization of vesicles from the RP by G85R-SOD1-YFP, but not by WT-SOD1-YFP.

Figure 3. Presynaptic infusion of G85R-SOD1 inhibited synaptic vesicle availability. Representative electron microscopy images illustrate morphology of active zones (AZs, labeled with red *) and numbers of synaptic vesicles (SVs) in fixed synapses infused with WT-SOD1 (A, $n = 3$) and G85R-SOD1 (B, $n = 3$). G85R-SOD1-infused synapses showed vacant active zones and occasional abnormal membranous structures (indicated by blue # and purple ^). (C-F) Quantification of averaged vesicle number across all AZs from 102 WT- and 102 G85R-SOD1-YFP-infused synapses showed statistically significant reductions in the total vesicle number and in the electron lucid vesicle number by G85R-SOD1-YFP as compared to WT-SOD1. The clathrin coated vesicles and the large electron lucid vesicles were comparable between WT and G85R-SOD1-YFP infused synapses. Nested one-way ANOVA was performed to compare WT and G85R infused synapses ($P<0.0001$) as well as across biological triplicates within each group ($P>0.05$). (G) Averaged number of SVs per AZ were plotted along the distance from

AZ (binned by 50nm). (H) Distance distribution plot of SVs in each 50µm bin showed a global reduction of SVs from G85R-SOD1-YFP infused synapses regardless of the distance from the AZs. Due to the drastically reduced numbers of SVs far (>675nm) from the AZs in both WT and G85R synapses, the reduction seemed to disappear or even be reversed, however, the differences far from the AZ may not be significant due to the substantially decreased numbers of vesicles in that area for both WT and G85R synapses. (I) Cumulative SV distribution plots showed similar distribution patterns of vesicles in WT (solid line) and G85R (dashed line) synapses, confirming the even inhibition of SV availability by G85R-SOD1 independent of the distance from the AZs.

Figure 4. Intermittent HFS (iHFS) prevented synaptic transmission deficits caused by G85R-SOD1-YFP. (A) iHFS (5 sec of 50 Hz applied every 30 min) was first applied to the synapse at time 0 before G85R injection, both pre- and post-synaptic membrane potentials were recorded 1min after HFS (P1). (B) If iHFS trains were applied every 30min before and during continuous SOD1-YFP infusion into the synapse, G85R-SOD1 no longer inhibited synaptic transmission and the synapse continued to fire even after 7 hours without significant changes in either pre- or post- synaptic potentials (P15) (C) EPSP slopes remained constant and comparable under basal stimulation with iHFS in WT and G85R-synapses. (D) EPSP slope from one single train of iHFS showed no significant difference between WT- and G85R-synapses except for occasional augmentation seen in G85R-SOD1-YFP-infused synapses. (E) To evaluate the vesicle dynamics, EPSP slopes were measured and integrated during HFS trains applied either with 2hr WT- or G85R-SOD1-YFP infusion in the presence of iHFS every 30 min ($n = 6$). There were no significant differences in RRP size and mobilization rate of vesicles trafficking from RP to RRP by G85R-SOD1-YFP. (F) EM showed normal presynaptic structure with normal numbers of vesicles at the active zone in G85R-SOD1-YFP-infused synapses when iHFS was applied. Interestingly, in 3 out of 5 synapses, HFS restored firing in G85R-SOD1-YFP-infused synapses, where EPSPs were significantly inhibited (Fig.4-1).

Figure 5. Presynaptic infusion of G85R-SOD1-His increased Ca^{2+} levels in the presynaptic terminal. Ratiometric live Ca^{2+} imaging was performed every 30sec after electrophoretic (100 nA current) infusion of a Ca^{2+} indicator, 1mM Fura-2 in 100mM KCl, into the presynaptic axon through the 1st presynaptic stimulation electrode inserted into the "palm" (Fig.1A). Fura-2 injection continued for 10min and the synapse was allowed to equilibrate for 30 min before SOD1 injection through the 2nd electrode to ensure Fura-2 was diffused evenly throughout the whole presynaptic terminal at roughly 100μM. Ratiometric images were taken at Ex360 nm and Ex390 nm assisted by ultra-high-speed wavelength switching Lambda DG-4/5 xenon arc lamp system. Ratios at various locations (A) were calculated as (fluorescent intensity^{360nm})/(fluorescent intensity^{390nm}) to provide a measure of intracellular Ca^{2+} concentrations. The blue arrow indicates the injection site for SOD1 proteins. 1: "Palm", 2-6: PreG, 4: Infusion site, 7: PreS. (B) G85R-SOD1-His induced Ca^{2+} increases while WT-SOD1-His had no effect on Ca^{2+} concentration. Raw Ca^{2+} concentrations were derived from the equation $[Ca^{2+}] = Kd'\ (R - Rmin)/(Rmax - R)$ and averaged across 12 WT- and 19 G85R-SOD1-injected presynaptic terminals (PreG) respectively. Kd′, Rmin and Rmax were calculated from standards as described in methods. Though different synapses varied in their baseline Ca^{2+} concentrations, G85R consistently increased $[Ca^{2+}]$ at around 60 min after protein injection whereas WT had no effect. (C-D) Baseline normalized Ca^{2+} ratio defined as $(R_{120}\text{-}R_0)/R_0$ (R_{120}: 60min after SOD1 injection, R_0: before SOD1 injection) were plotted at 4 sites for WT (n=12) and G85R (n=19). G85R-SOD1 caused increases in $[Ca^{2+}]$ at all sites including the "palm" where Ca^{2+} channels are sparse or absent. The increase in $[Ca^{2+}]$ correlated roughly with G85R-SOD1 concentration, with the highest levels at the injection site and lowest in PreS, a smaller presynaptic axonal branch infused with fura-2 at a comparable concentration but with a lower SOD1 concentration due to slower diffusion from the injection site in PreG. (E-F) iHFS applied at 30 min after SOD1 injection seemed to restore Ca^{2+} homeostasis in G85R-SOD1-injected synapses (*n = 19*) and this equilibrium lasted at least 2 hours after iHFS, similar to that in WT (*n = 12*), this suggested the possibility that redistribution of Ca^{2+} is induced by iHFS. As expected, Ca^{2+} levels increased during HFS in synapses infused with either WT or G85R-SOD1 proteins (Fig. 5-1).

833

834 **Figure 6. EGTA, a Ca^{2+} chelator, prevented G85R-SOD1-YFP-induced synaptic dysfunctions.** (A)
835 EPSP slopes of 6 double injected synapses (50mM EGTA and 50μM G85R-SOD1-YFP) were plotted
836 from 30 min before the injection to 2 hours after the injection. There was no reduction in EPSP slopes
837 with EGTA and G85R-SOD1-YFP in contrast to that seen in synapses injected with G85R-SOD1-YFP
838 alone (*n = 8*) or WT-SOD1-YFP alone (*n = 5*), data for G85R- and WT-SOD1 from Figure 1C is
839 included for comparison. All EPSP slopes were averaged and plotted with error bars indicating standard
840 error (for unnormalized data, see Fig. 6-1). (B) Ratiometric Fura-2 Ca^{2+} imaging showed comparisons of
841 Ca^{2+} concentrations in the presynaptic terminals (PreG) injected with WT-SOD1, G85R-SOD1, and
842 G85R-SOD1+ EGTA, EGTA prevented the Ca^{2+} increase caused by G85R-SOD1 (*n = 4*). Due to the
843 chelating effect of EGTA, the basal level of Ca^{2+} decreased over time during co-infusion of G85R and
844 EGTA. (C) Normalized ratios (subtracting levels with EGTA alone), positively correlated with Ca^{2+}
845 concentrations, showed constant basal Ca^{2+} levels at various presynaptic regions injected with G85R-
846 SOD1 in the presence of EGTA. (D) EPSP slopes from synapses injected with EGTA and G85R-SOD1
847 were integrated, normalized to the initial time point before the injection, and fit linearly to show RRP size
848 as indicated by the intersection with the Y axis and the vesicle mobilization rate from RP to RRP as
849 indicated by the slope of the linear fit. Compared with WT-SOD1-injected synapses (green) and synapses
850 before injections (black), EGTA+G85R-SOD1-injected synapses showed little change in the RRP size
851 and the mobilization 120 min after injection (red) and 180 min after injection (blue). (E) Quantification of
852 RRP size and mobilization for synapses injected with WT-SOD1 (*n = 11*), or G85R-SOD1 (*n = 6*), or
853 G85R-SOD1 + EGTA (*n = 5*) showed that EGTA prevented the decreases in RRP size and mobilization
854 rate caused by G85R-SOD1-YFP. Error bars indicate standard error. (F) Representative EM image
855 showed abundant synaptic vesicles at the active zone of a synapse injected with EGTA and G85R-SOD1-
856 YFP. (G) EGTA restored the synaptic vesicle numbers to normal at the active zones (*102* active zones
857 from 3 independent experiments for each group).

858

EXTENDED DATA

Figure 1-1. No effects of fluorescent dextran on synaptic transmission. Synapses infused with rhodamine-dextran alone kept firing for >2hr, without significant changes in synaptic strength as evidenced by constant postsynaptic membrane potential waveform (A) and EPSP slope (B).

Figure 1-2. Recovery of synaptic transmission after the removal of G85R-SOD1-YFP. The synapse was injected with G85R-SOD1-YFP continuously for 30 min till the significant reduction in EPSP slope and the failure to elicit a postsynaptic action potential. As the injection stopped, G85R-SOD1-YFP slowly diffused away from the presynaptic terminal to the axon, leading to a full recovery of EPSP after 150 min, suggesting that synaptic machinery remained intact after treatment. After the synapse and neurotransmission were stabilized for more than 1 hour, G85R-SOD1-YFP was injected again and a similar inhibitory effect was observed.

Figure 2-1. Significant inhibition of EPSP by continuous HFS in G85R-SOD1-YFP-infused synapse. EPSP slopes taken during the 6^{th} train in a set of continuous trains of HFS showed even more dramatic decreases by G85R-SOD1-YFP, compared with the WT-SOD1-YFP, particularly at the beginning, suggesting limited synaptic vesicle availability, consistent with the morphological changes found in EM. Note that in panel 2A, the EPSP slope with G85R-SOD1-YFP in the 1^{st} train was initially >150, while in the 6^{th} train, it never got above 40. In contrast, the initial EPSP slopes in the 1^{st} train and the 6^{th} train were almost identical after perfusion with WT-SOD1-YFP.

Figure 4-1. Rescuing effects of HFS in dying synapses. In 3 out of 5 synapses where the EPSP slopes were significant inhibited by G85R-SOD1-YFP but were still above 50, one train of HFS surprisingly restored neurotransmission as indicated by the rescue of EPSP slope. Synaptic membrane potentials were measured in pre- and post-synaptic terminals before G85R-SOD1 infusion (A), after inhibition (B), and after one train of HFS (C). HFS partially restored the RRP size without rescuing vesicle mobilization rate

885 in these synapses. In the other 2 synapses where EPSP slopes had dropped below 50, a train of HFS
886 further decreased the EPSP slope to almost 0, consistent with its role in depleting RRP.
887
888 **Figure 5-1. Increases in Ca^{2+} levels under HFS.** Synapses infused with WT-SOD1 (A) of G85R-SOD1
889 (B) exhibited increased Ca^{2+} levels upon HFS, mainly in the presynaptic terminals, with comparable
890 changes at the protein infusion site and the rest of the terminal (PreG). The "Palm", which lacks Ca^{2+}
891 channels didn't show changes in Ca^{2+} influx, consistent with previous findings. G85R-SOD1 didn't seem
892 to alter the overall pattern, except for larger fluctuations particularly at the "Palm" and the protein
893 infusion site, which may indicate changes in Ca^{2+} homeostasis independent of Ca^{2+} channels.
894
895 **Figure 6-1. Unnormalized EPSP slopes.** EPSP slopes were measured and plotted without normalization
896 for synapses infused with WT-SOD1-YFP (A), G85R-SOD1-YFP (B), and G85R-SOD1-YFP + EGTA
897 (C)
898
899 **MULTIMEDIA, FIGURE, and TABLE**

Figure 1

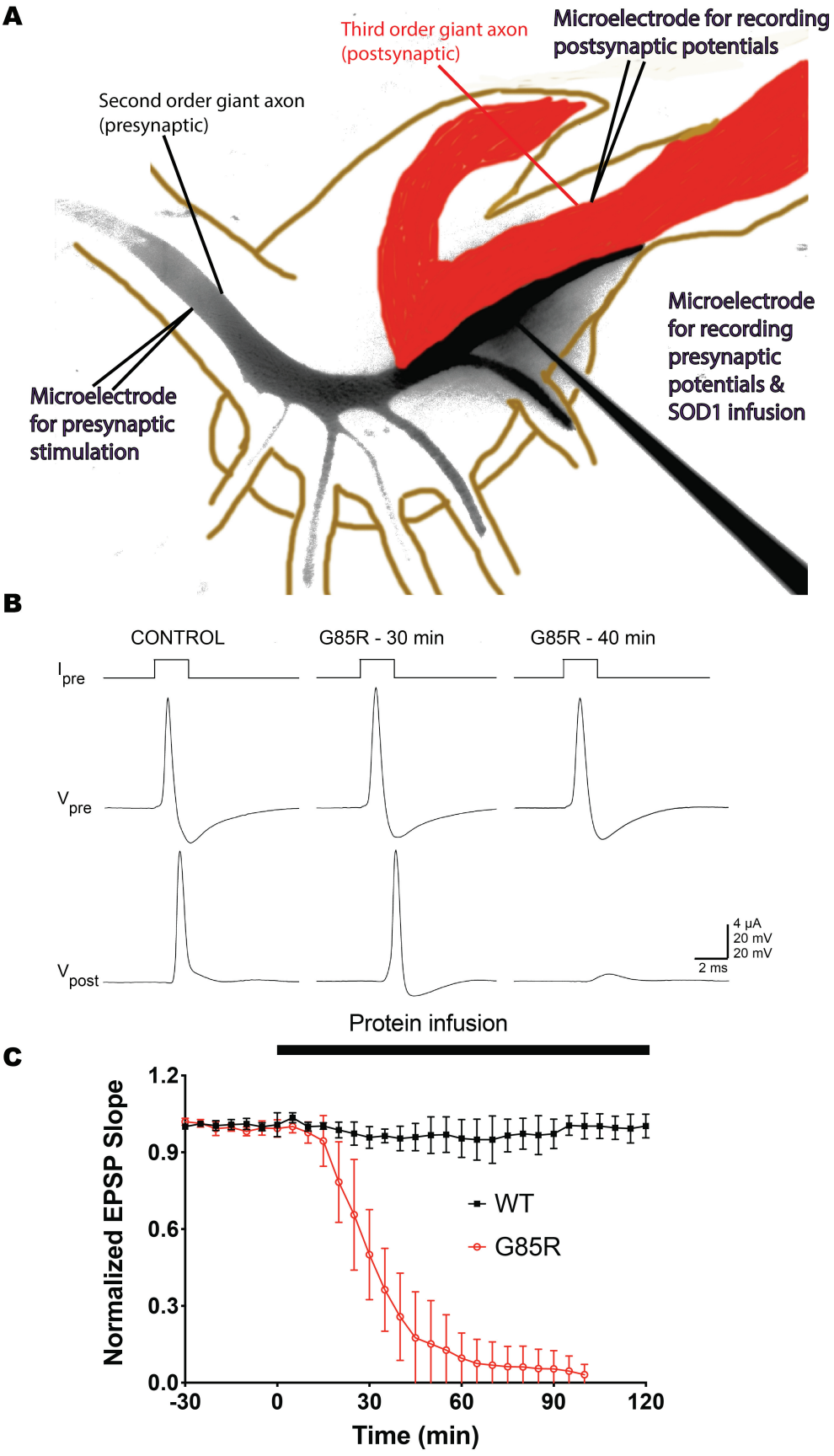

Figure 2

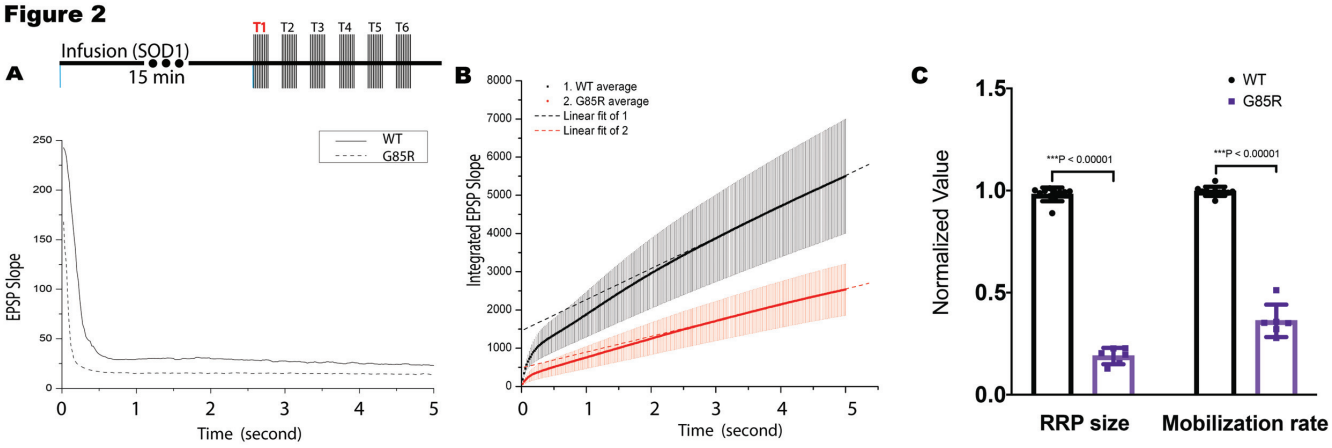

Figure 3

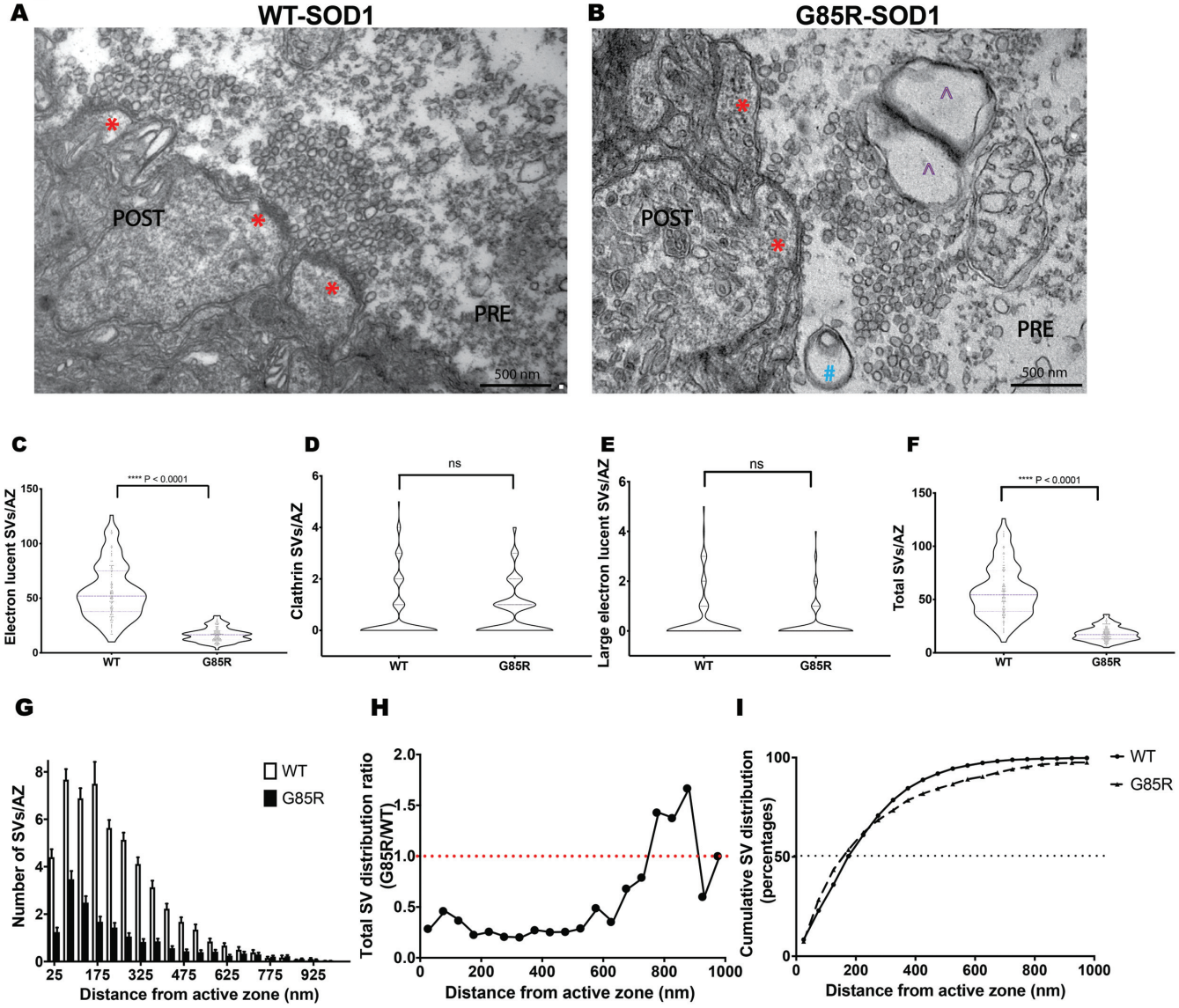

Figure 4

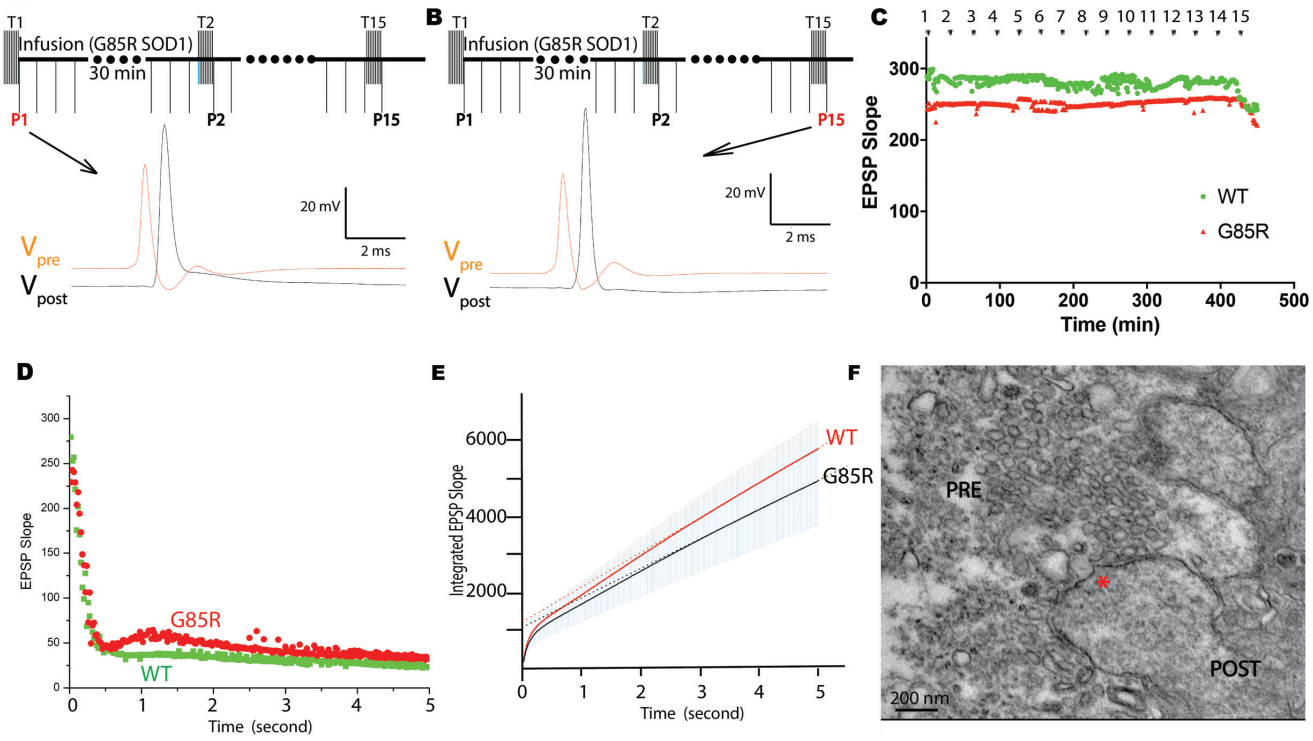

Figure 5

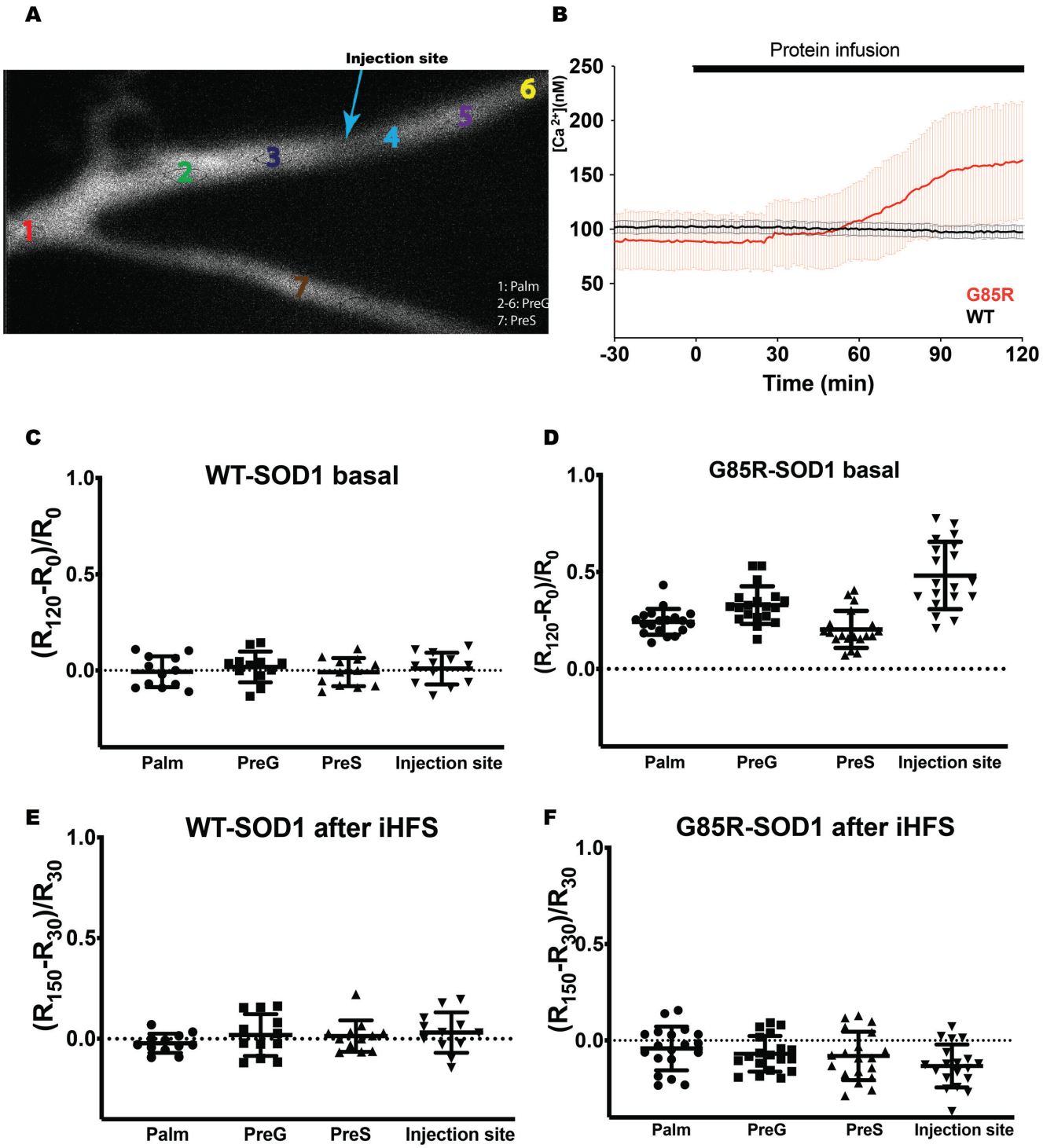

Figure 6